nature geoscience

ARTICLES

https://doi.org/10.1038/s41561-021-00813-1

Rapid and sensitive response of Greenland's groundwater system to ice sheet change

Lillemor Claesson Liljedahl[1,9]✉, Toby Meierbachtol[2]✉, Joel Harper[2], Dirk van As[3,4], Jens-Ove Näslund[1], Jan-Olof Selroos[1], Jun Saito[2], Sven Follin[5], Timo Ruskeeniemi[6], Anne Kontula[7] and Neil Humphrey[8]

Greenland Ice Sheet mass loss is impacting connected terrestrial and marine hydrologic systems with global consequences. Groundwater is a key component of water cycling in the Arctic, underlying the 1.7e^6 km^2 ice sheet and forming offshore freshwater reserves. However, despite its vast extent, the response of Greenland's groundwater to ongoing ice sheet change is unknown. Here we present in-situ observations of deep groundwater conditions under the Greenland Ice Sheet, obtained in a 651-metre-long proglacial bedrock borehole angled under the ice sheet margin. We find that Greenland's groundwater system responds rapidly and sensitively to relatively minor ice sheet forcing. Hydraulic head clearly varies over multi-annual, seasonal and diurnal timescales, which we interpret as a response to fluid pressure forcing at the ice/bed interface associated with changes in overlying ice loading and ice sheet hydrology. We find a systematic decline in hydraulic head over the eight-year observational period is linked primarily to ice sheet mass loss. Ongoing and future ice thinning will probably reduce groundwater discharge rates, with potential impacts to submarine freshwater discharge, freshwater delivery to fjords and biogeochemical fluxes in the Arctic.

The present-day Greenland Ice Sheet (GrIS) plays a central role in the flows of water, energy and solutes across the Arctic due to its size and coupling to the atmosphere, marine, periglacial and groundwater systems. Substantial systems-wide change is underway in the Arctic, driven by rapid warming[1]. The GrIS is in a state of mass loss[2] and geometric evolution[3], permafrost regions are warming[4,5] and ocean salinity[6,7] and sea-ice cover[8] are shifting and declining. Feedbacks and interactions of these changing environmental conditions can be expected to eventually impact all aspects of hydrologic processes, including the expansive groundwater system of Greenland.

A longstanding paradigm is that at the bed of ice sheets, loading from thick ice drives water into a regional groundwater flow field, recharging beneath the ice and discharging to the proglacial terrestrial surface and/or surrounding ocean floor[9–11]. Supporting measurements of a groundwater system forced by ice sheets are unfortunately almost exclusively limited to areas that experienced glacial conditions many thousands of years ago[12], where constraints on the palaeo ice-sheet geometry, permafrost and groundwater systems are retrospective and cannot be validated. Until now, there have been no concurrent measurements of ice sheet and underlying groundwater hydrologic conditions. Testing of fundamental concepts has therefore been limited to numerical modelling studies (for example, refs. [9–11]), which have primarily considered coarse temporal and spatial scales.

A clear disconnect has emerged between the timescales guiding the paradigm of ice sheet/groundwater coupling and those associated with rapid ice sheet change. The fluxes of groundwater in both Arctic and Antarctic settings indicate such a disconnect is consequential for constraining changes in water cycling controlled by ice sheets. High fluxes of submarine groundwater discharge driven by ice sheets have been measured off the coast of Antarctica[13], which modelling suggests may contribute one third of the freshwater flux to the ocean in places adjacent to the ice sheet[14]. The groundwater system may in fact be a key component of Antarctica's subglacial hydrologic system and flow dynamics[15]. Although there are no direct measurements of submarine discharge from the GrIS, the only study so far estimated fluxes of ~30 Gt yr^{-1}, forced regionally by the ice sheet[11]. The sensitivity of Greenland's groundwater system to present warming-driven changes to the ice sheet are unclear, but the consequences for water exchange between groundwater, adjacent terrestrial and ocean systems and the ice sheet itself are potentially great.

No existing study of current or palaeo ice sheets provides observational evidence to address the sensitivity of groundwater systems to ice sheet forcing at the seasonal to decadal timescales shaping the present-day Arctic. We address this problem through new direct measurements of groundwater system change beneath an active ice sheet, concurrent with observations of ice sheet hydrologic and ice flow forcing processes.

Concurrent groundwater and ice sheet measurements

In 2011, we completed an angled (70°) proglacial bedrock borehole (DH-GAP04) to a depth of 651 m below the ground surface, ending under Isunnguata Sermia, a land-terminating outlet of the ice sheet in southwest Greenland (Fig. 1). The outlet has large gradients in ice thickness ranging from <100 m near the ice edge to 900 m or more along the glacier centerline 3 km from the margin. Measurements on the ice sheet were also collected at four sites ~15–35 km from the bedrock hole (Fig. 1) to establish the hydrologic[16] and ice flow[17]

[1]Svensk Kärnbränslehantering AB, Solna, Sweden. [2]Department of Geosciences, University of Montana, Missoula, MT, USA. [3]Geological Survey of Denmark and Greenland, Copenhagen, Denmark. [4]Greenland Guidance, Utrecht, the Netherlands. [5]Golder Associates AB, Stockholm, Sweden. [6]Geological Survey of Finland, Espoo, Finland. [7]Posiva Oy, Eurajoki, Finland. [8]Department of Geology and Geophysics, University of Wyoming, Laramie, WY, USA. [9]Present address: DHI, Stockholm, Sweden. ✉e-mail: lcla@dhigroup.com; toby.meierbachtol@umontana.edu

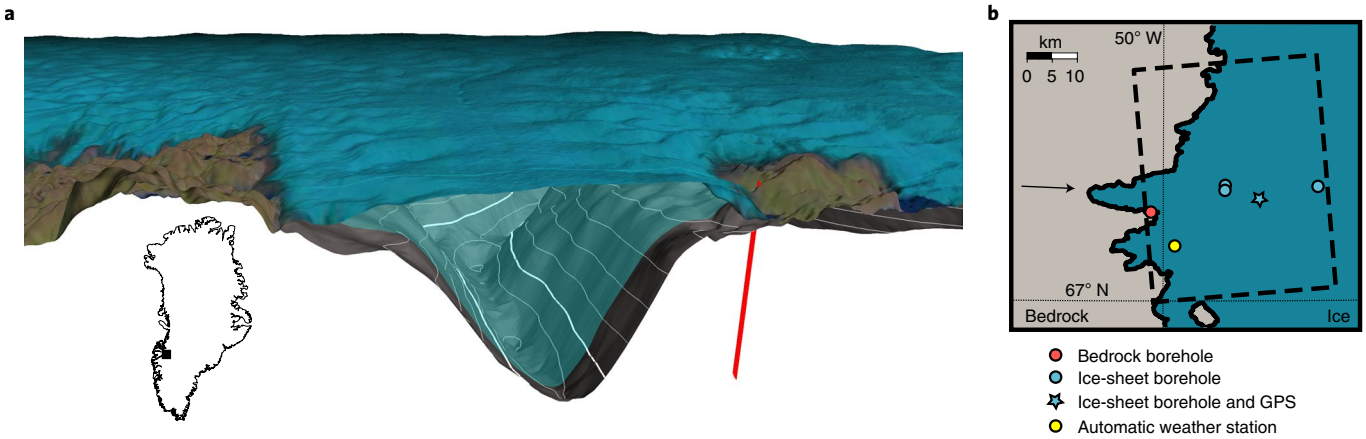

Fig. 1 | Local and regional site setting. a, Three-dimensional view of bedrock borehole (red line) adjacent to the Isunnguata Sermia outlet glacier (cut out). Contours delineate ice sheet bed topography at 100 m intervals, with zero-metre contour shown in thick white. LandSAT image (July 2020) is draped over surface and proglacial topography. Blue transparent shading illustrates cross-section cut out extending from the bedrock borehole across the Isunnguata Sermia trough outlet. Topography is vertically exaggerated (5×) for visual clarity. **b**, Regional site setting. The blue star indicates the location of the ice velocity and surface melt data presented in Fig. 3c. Full extent of imagery in **a** is shown by dashed box in **b**, with arrow indicating the look direction in **a**.

setting in support of groundwater observations. These data include basal water pressure measured in a network of 32 boreholes drilled to the ice sheet bed[16].

The bedrock borehole penetrated fractured Archaean gneiss[18], which is characteristic of the region's proglacial[19] and subglacial[20] geology. Permafrost is observed along the borehole to a depth of nearly 400 m (Fig. 2), consistent with the area's continuous proglacial permafrost structure. Measurements of thermal conditions at the ice sheet bed in the study area[21] support the prevailing view that the western GrIS is warm based[22]. Extension of deep frozen bedrock conditions under the ice is possible, but probably restricted to a relatively thin zone along the margin[23]. Hydraulic testing after drilling indicated fracture networks with variable hydraulic characteristics[18] (Fig. 2 and Extended Data Table 1; Methods). Based on these findings, instrument clusters were installed in three packed off, and hence isolated, sections: upper (400–561 m; 'Up'), middle (561–571 m; 'Mid') and lower (571–651 m; 'Low'). Absolute pressure was measured in each section at 1–4 hour intervals and converted to hydraulic head (Supplementary Methods), yielding a unique, eight-year record of groundwater head at high temporal resolution in fractured bedrock with hydraulic transmissivity spanning two orders of magnitude.

Three timescales of groundwater change

The bedrock borehole reveals systematic groundwater head changes at diurnal, seasonal and multi-annual timescales (Figs. 2 and 3). Groundwater heads in sections Up and Mid show connected behaviour and can be interpreted effectively as a single bedrock aquifer, with heads nominally 30 m greater than the heads in section Low. Nevertheless, seasonal variability superimposed on a long-term trend of declining head is characteristic of all sections over the eight-year period. Over the full observational record, heads declined by 7.9 m (Low) to 12.6 m (Up); equivalent to −1.0 to −1.5 m yr^{-1}.

The annual pattern of head swings is remarkably consistent each year, with seasonal oscillations of nearly 10 m in amplitude in the Up/Mid sections (Fig. 2). Heads reach an annual minimum each autumn, and steadily increase over winter. The rate of head rise suddenly increases in spring, leading to maximum head values in mid-summer and a subsequent rapid decline until early/late autumn. The largest head increase occurs during winter (3.8–7.0 m), which is the longest seasonal period of the annual cycle (118–200 days). Seasonal swings are also observed in section Low, but with smaller magnitudes (<2 m). Superimposed on the seasonal cycle are daily head variations (Fig. 3). Diurnal and semi-diurnal head cycles occur year-round, typical of Earth tide forcing[24]. However, smooth diurnal cycles develop as groundwater head peaks during summer and are amplified by a factor of 3–4 compared with winter (Fig. 3): behaviour that cannot be attributed to Earth and ocean tidal signals (Supplementary Discussion). The peak diurnal range reaches 0.15 m in late summer.

Ice sheet forcing on the groundwater system

Fluxes of meltwater and thinning/thickening of the overlying ice sheet act as boundary forcings on the groundwater system by limiting water available for recharge, setting fluid pressure conditions at the ice/earth boundary[25] and/or by introducing a transient load that drives volumetric perturbations of the bedrock's aquifer framework[26]. We find that effects of glaciological processes on fluid pressure are most closely linked to the magnitudes, intervals and timing of groundwater head variations over the three timescales we identify. Fluid pressure conditions beneath the GrIS are determined by a combination of the overburden ice load and an evolving subglacial drainage system. Variability in ice dynamics and surface mass balance cause ice thickness changes that set the overburden load and, at the ice sheet bed, continuous adjustment of water-routing pathways in response to changing meltwater fluxes generates variable basal pressures that are rarely equal to ice overburden. These time-varying glaciological processes are highly sensitive to the presence/absence of ice sheet surface melt (for example, ref. [27]).

The observed long-term decline in groundwater head is commensurate with nearby thinning of the ice sheet. Ice adjacent to the bedrock borehole has thinned at a mean rate of ~1.3 m yr^{-1} water equivalent during the 2011–2019 observational period (Fig. 3; Methods). As detailed below, drainage system processes generate characteristic seasonal water pressure variability, but the agreement between ice thinning and groundwater head decline over longer multi-annual timescales suggests that any changes in basal pressure from long-term evolution of the drainage system are second order compared with reductions in load from thinning (Fig. 4).

Seasonally, our data identify ice sheet processes that are also consistent with groundwater head variations. During winter, ice thickness steadily increases from ice flow. During the melt season, high surface melt rates cause a transition to ice thinning, despite accelerating velocities (Fig. 3; Methods). This seasonal loading cycle is

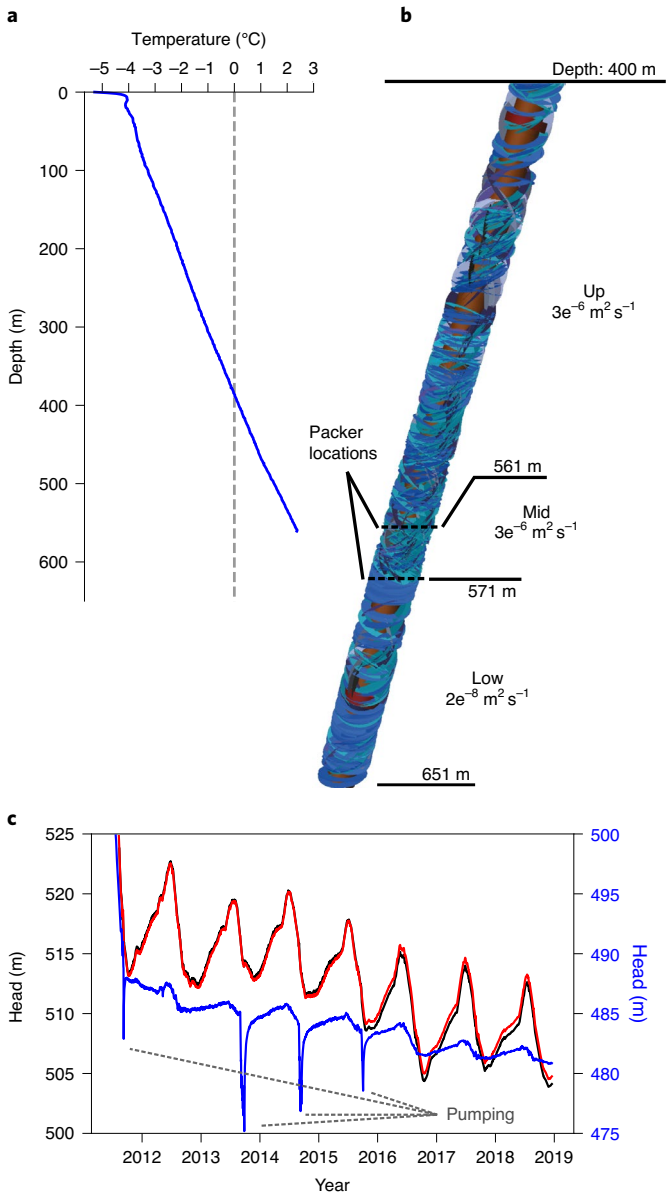

Fig. 2 | Bedrock borehole measurements of physical setting and groundwater head. a, Bedrock temperature (Supplementary Methods). **b**, Visual log of borehole fracture detail from 400 m depth, below the permafrost base, to borehole bottom. Borehole trajectory is shown in brown, and fractures are illustrated in blue/purple (different shading is for visual effect). Packer locations are indicated by black dashed lines. Borehole sections are indicated along with section hydraulic transmissivities (the sum of all PFL transmissivities calculated in each section; $m^2\ s^{-1}$), and borehole depths are indicated with black lines (m). **c**, Eight years of groundwater head measured in sections Up (black), Mid (red) and Low (blue). Low section head is referenced to right *y* axis. Artificial head disturbances from periodic borehole pumping are noted.

consistent with the seasonal groundwater head cycle, with differences in the timing and details of groundwater change that are qualitatively consistent with measured basal pressures and the understanding of processes occurring in the basal drainage system. In spring, the onset of ice surface melt induces high basal water pressure[16] that peaks during summer. Similarly, in each year of measurement the spring acceleration in groundwater head increase occurs within days of surface melt onset (Fig. 3 and Extended Data Fig. 1). Later in summer, increasing efficiency of the basal drainage network leads to lower spatially averaged pressures[28,29] and large diurnal pressure variations (Fig. 3) as the system routes meltwater fluxes with magnitudes that follow the daily melt cycle. This too is consistent with the diurnal variations in the groundwater record, which are amplified after seasonal head peaks and begin to decline in mid-summer.

Our interpretation that groundwater head responds to fluid pressure changes at the ice/earth boundary is further supported by evidence that the groundwater system does not respond to water recharge limitations or solid earth deformation. First, we expect groundwater heads would closely relate to seasonal variations in ice sheet runoff if recharge was limited by subglacial water flux. Yet, peak groundwater heads in summer typically precede maximum runoff by up to eight weeks, and the magnitude of groundwater head rise is unrelated to the peak runoff value (Extended Data Fig. 1). Groundwater heads climb each winter despite no surface melt input, and water is known to discharge from the ice sheet terminus in winter, indicating excess basal water[30]. Not only is the timing incongruent with a flux forcing on recharge, but the ice sheet bed is never water limited for recharge. Second, hydromechanical loading of the aquifer framework should induce larger groundwater head changes in conditions of low aquifer permeability[31] if this process is the primary cause of head change. But, our measurements show that the magnitude of seasonal head change in sections Up/Mid are greater than in section Low by a factor of 3–4, despite transmissivities that are two orders of magnitude larger (Fig. 2). This suggests that the measured groundwater seasonality does not reflect a response to elastic earth deformation from ice loading.

Fracture networks intersected by the borehole along its length can be expected to connect to and sample conditions across different regions of the ice sheet bed. Indeed, our measurements suggest that the spatial footprint of ice sheet forcing on the groundwater system varies with depth along the borehole, with section Low probably demonstrating a more remote connection, perhaps as far as the deep subglacial trough, whereas sections Up/Mid are probably connected to closer and shallower ice (Fig. 4 and Extended Data Fig. 2; Supplementary Discussion). The precise footprints cannot be determined, and interpretations are additionally complicated by the different borehole section transmissivities. The different hydraulic characteristics probably play a role in the muted seasonal and long-term head response in section Low (compared with sections Up/Mid), since the attenuation of a perturbation is inversely related to aquifer transmissivity (for example, ref. [32]).

The complexities of the fractured bedrock site and the spatial limitations of our ice sheet data present a challenge to generating a specific, measurement-based partitioning of the seasonal ice processes driving groundwater heads. Despite these complications, the consistency between observed groundwater heads and seasonal ice loading and drainage processes determining subglacial fluid pressure is clear. Moreover, the declining heads over eight years in a groundwater system with hydraulic transmissivities spanning orders of magnitude demonstrate strong sensitivity to the ice sheet's recent trend of mass loss. In fact, mass loss and associated thinning has been ongoing in the region for more than 20 years[33]. Based on the observed deep groundwater response to forcing over daily to multi-annual timescales, the perturbation from longer, multi-decadal ice thinning has probably propagated many tens of kilometres in the groundwater system (Methods).

Implications for connected systems

The seasonal ice sheet processes at our site align with the glaciological paradigms for basal drainage system and ice flow response to surface melting across the GrIS's widespread ablation zone. Basal water pressures evolve in response to surface melt across several tens of kilometres of the outer ablation zone[16,27,28,34], and ice flow

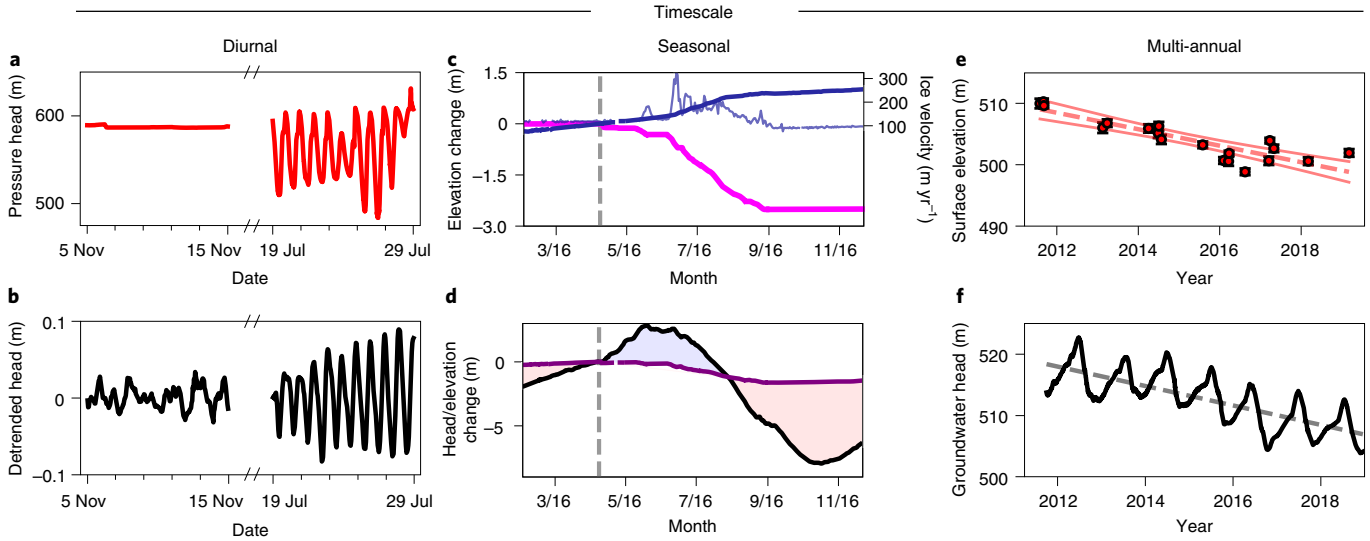

Fig. 3 | Three timescales of ice sheet forcing and groundwater response. a,**b**, Diurnal subglacial water pressure (**a**; red) and groundwater head (**b**; black) during winter and summer periods. Groundwater head has been detrended for clarity. Measurements are from 2012 (subglacial water pressure; **a**) and 2016 (groundwater head; **b**) to exemplify characteristic behaviour rather than connected forcing and response. **c**, Seasonal surface mass balance (magenta) and ice flow (thick blue line) components contributing to ice surface elevation change from date of melt onset (8 April 2016; dashed grey line) (Methods). The thin blue line shows measured ice velocity for reference (right *y* axis). **d**, Surface elevation change resulting from seasonal surface mass balance and ice flow in **c** (purple) and change in section Up groundwater head (black). Red (blue) shaded regions reflect periods where subglacial water pressure must be less (greater) than the pressure on the day of melt onset to bring ice sheet forcing into general agreement with groundwater response curve. **e**,**f**, Multi-annual ice sheet surface elevation change near the bedrock borehole (**e**) and groundwater head (**f**) in section Up. Dashed lines in **e** and **f** show least squares linear regressions and thin red lines in **e** indicate 95% confidence intervals. Timescales are grouped by column.

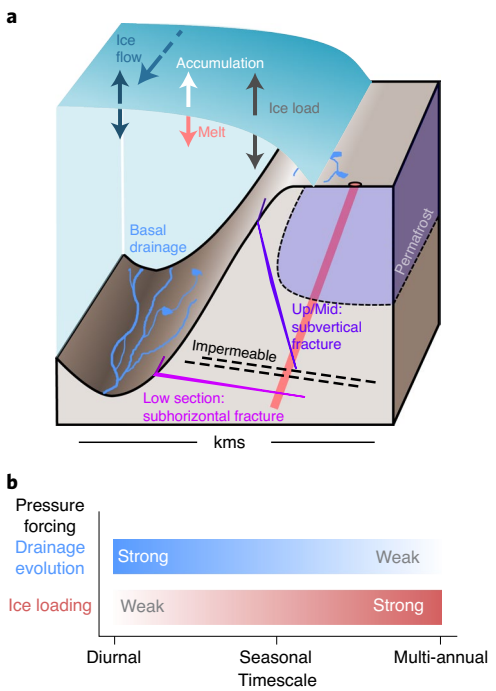

Fig. 4 | Data-driven conceptualization. a, Site conceptualization of ice sheet processes forcing groundwater response and interpreted connectivity of the borehole to regions of the ice sheet bed based on measured fracture characteristics, groundwater head and plausible hydraulic heads at the ice/bed boundary (Supplementary Discussion). **b**, Conceptual diagram of the relative strength of basal drainage and ice loading processes at different timescales.

seasonally accelerates/decelerates across the entire ablation zone[35,36]. Recent decadal trends have been toward intensifying melt, a longer melt season and inland expansion of melt intensity[37] around the ice sheet. This has had consequences for the seasonal evolution of the drainage system and ice flow[36]. As these processes continue to adjust to a warming climate, corresponding impacts to the groundwater system can be expected.

The reduction in groundwater head from thinning ice around the GrIS's periphery is likely to reduce head gradients along the ice sheet margins, where marine and terrestrial (for example, taliks) water levels are essentially fixed (compared with rates of ice sheet thinning). A commensurate reduction in groundwater exchange with periglacial and marine systems can be expected, and our findings suggest that this occurs without delay. The mass loss near our site during the past decades is consistent with, and in fact less than, many other regions of the ice sheet[33]; particularly, marine-terminating outlets where dynamical ice thinning has often exceeded 100 m and propagated inland many tens of kilometres in recent decades[38]. Thus, reductions in groundwater flux are probably ubiquitous around the GrIS, with some regions impacted more than our measurements and interpretations indicate. The reduced groundwater flux would result in increased flow through the subglacial drainage system.

In this context, our finding of a tight coupling between groundwater and the changing GrIS has potentially far-reaching and impactful implications for coupled Arctic systems. For example, seasonal cycling and long-term reductions in fresh groundwater discharge to Greenland's fjord walls and floors may play a role in the heat and salinity fluxes known to drive marine circulation, ice melting and calving of marine glacier termini[39,40]. Additionally, polar ice sheets generate high rates of biogeochemical and physical weathering[41], and large solute and methane fluxes in submarine groundwater seeps have been associated with glacier forcing elsewhere in the Arctic[42]. A dynamic groundwater system may therefore

be important to assessments of the storage and cycling of chemical constituents, organic carbon and microbial life under warming climate conditions.

As the ice sheet rapidly adjusts to a warming climate, groundwater head and head gradient responses can be expected to quickly propagate ice sheet change to coupled hydrologic systems. We observe a groundwater system that responds to multi-annual, seasonal and even daily perturbations from the overlying ice sheet. This response timescale is orders of magnitude shorter than is implemented in models. Such tight and sensitive coupling between ice sheet and groundwater potentially touches many aspects of the Arctic, and requires quantification of the water and chemical fluxes across systems.

Online content

Any methods, additional references, Nature Research reporting summaries, source data, extended data, supplementary information, acknowledgements, peer review information; details of author contributions and competing interests; and statements of data and code availability are available at https://doi.org/10.1038/s41561-021-00813-1.

Received: 3 November 2020; Accepted: 13 July 2021;
Published online: 23 September 2021

References

1. Meredith, M. et al. in *Special Report on the Ocean and Cryosphere in a Changing Climate* (eds Pörtner, H.-O. et al.) (IPCC, 2019)
2. Shepherd, A. et al. Mass balance of the Greenland Ice Sheet from 1992 to 2018. *Nature* **579**, 233–239 (2020).
3. Smith, B. et al. Pervasive ice sheet mass loss reflects competing ocean and atmosphere processes. *Science* **368**, 1239–1242 (2020).
4. Romanovsky, V. E., Smith, S. L. & Christiansen, H. H. Permafrost thermal state in the polar Northern Hemisphere during the International Polar Year 2007–2009: a synthesis. *Permafr. Periglac. Process.* **21**, 106–116 (2010).
5. Biskaborn, B. K. et al. Permafrost is warming at a global scale. *Nat. Commun.* **10**, 264 (2019).
6. Carmack, E. C. et al. Freshwater and its role in the Arctic marine system: sources, disposition, storage, export, and physical and biogeochemical consequences in the Arctic and global oceans. *J. Geophys. Res. Biogeosci.* **121**, 675–717 (2016).
7. Bamber, J. L. et al. Land ice freshwater budget of the Arctic and North Atlantic Oceans: 1. data, methods, and results. *J. Geophys. Res. Oceans* **123**, 1827–1837 (2018).
8. Stroeve, J. & Notz, D. Changing state of Arctic sea ice across all seasons. *Environ. Res. Lett.* **13**, 103001 (2018).
9. Lemieux, J.-M., Sudicky, E. A., Peltier, W. R. & Tarasov, L. Dynamics of groundwater recharge and seepage over the Canadian landscape during the Wisconsinian glaciation. *J. Geophys. Res.* **113**, F01011 (2008).
10. Bense, V. F. & Person, M. A. Transient hydrodynamics within intercratonic sedimentary basins during glacial cycles. *J. Geophys. Res. Earth Surf.* **113**, F04005 (2008).
11. Defoor, W. et al. Ice sheet-derived submarine groundwater discharge on Greenland's continental shelf. *Water Resour. Res.* **47**, W07549 (2011).
12. Neuzil, C. E. & Provost, A. M. Ice sheet load cycling and fluid underpressures in the Eastern Michigan Basin, Ontario, Canada. *J. Geophys. Res. Solid Earth* **119**, 8748–8769 (2014).
13. Uemura, T., Taniguchi, M. & Shibuya, K. Submarine groundwater discharge in Lützow-Holm Bay, Antarctica. *Geophys. Res. Lett.* **38**, L08402 (2011).
14. Null, K. A. et al. Groundwater discharge to the western Antarctic coastal ocean. *Polar Res.* **38**, 3497 (2019).
15. Christoffersen, P., Bougamont, M., Carter, S., Fricker, H. & Tulaczyk, S. Significant groundwater contribution to Antarctic ice streams hydrologic budget. *Geophys. Res. Lett.* **41**, 2003–2010 (2014).
16. Wright, P. J., Harper, J. T., Humphrey, N. F. & Meierbachtol, T. W. Measured basal water pressure variability of the western Greenland Ice Sheet: implications for hydraulic potential. *J. Geophys. Res. Earth Surf.* **121**, 1134–1147 (2016).
17. Maier, N., Humphrey, N., Harper, J. & Meierbachtol, T. Sliding dominates slow-flowing margin regions, Greenland Ice Sheet. *Sci. Adv.* **5**, eeaw5406 (2019).
18. Claesson Liljedahl, L. et al. *The Greenland Analogue Project: Final Report* TR-14-13 (Svensk Kärnbränslehantering AB, 2016).
19. Engström, J. & Klint, K. E. S. Continental collision structures and post-orogenic geological history of the Kangerlussuaq area in the southern part of the Nagssugtoqidian orogen, central west Greenland. *Geosciences* **4**, 316–334 (2014).
20. Harper, J. T., Humphrey, N. F., Meierbachtol, T. W., Graly, J. A. & Fischer, U. H. Borehole measurements indicate hard bed conditions, Kangerlussuaq sector, western Greenland Ice Sheet. *J. Geophys. Res. Earth Surf.* **122**, 1605–1618 (2017).
21. Harrington, J. A., Humphrey, N. F. & Harper, J. T. Temperature distribution and thermal anomalies along a flowline of the Greenland Ice Sheet. *Ann. Glaciol.* **56**, 98–104 (2015).
22. Macgregor, J. A. et al. A synthesis of the basal thermal state of the Greenland Ice Sheet. *J. Geophys. Res. Earth Surf.* **121**, 1328–1350 (2016).
23. Ruskeeniemi, T. et al. Subglacial permafrost evidencing re-advance of the Greenland Ice Sheet over frozen ground. *Quat. Sci. Rev.* **199**, 174–187 (2018).
24. Nyberg, G., Jönsson, S. & Wass, E. *Äspö Hard Rock Laboratory Hydro Monitoring Program: Report for 2004* IPR-05-26 (SKB, 2005).
25. Person, M., Bense, V., Cohen, D. & Banerjee, A. Models of ice-sheet hydrogeologic interactions: a review. *Geofluids* **12**, 58–78 (2012).
26. Neuzil, C. E. Hydromechanical coupling in geologic processes. *Hydrogeol. J.* **11**, 41–83 (2003).
27. Andrews, L. C. et al. Direct observations of evolving subglacial drainage beneath the Greenland Ice Sheet. *Nature* **514**, 80–83 (2014).
28. Hoffman, M. J. et al. Greenland subglacial drainage evolution regulated by weakly-connected regions of the bed. *Nat. Commun.* **7**, 13903 (2016).
29. Werder, M. A., Hewitt, I. J., Schoof, C. G. & Flowers, G. E. Modeling channelized and distributed subglacial drainage in two dimensions. *J. Geophys. Res. Earth Surf.* **118**, 2140–2158 (2013).
30. Pitcher, L. H. et al. Direct observation of winter meltwater drainage from the Greenland Ice Sheet. *Geophys. Res. Lett.* **47**, e2019GL086521 (2020).
31. Neuzil, C. E. Abnormal pressures as hydrodynamic phenomena. *Am. J. Sci.* **295**, 742–786 (1995).
32. Rotzoll, K., Gingerich, S. B., Jenson, J. W. & El-Kadi, A. I. Estimating hydraulic properties from tidal attenuation in the Northern Guam Lens Aquifer, territory of Guam, USA. *Hydrogeol. J.* **21**, 643–654 (2013).
33. Mouginot, J. et al. Forty-six years of Greenland Ice Sheet mass balance from 1972 to 2018. *Proc. Natl Acad. Sci. USA* **116**, 9239–9244 (2019).
34. Meierbachtol, T., Harper, J. & Humphrey, N. Basal drainage system response to increasing surface melt on the Greenland Ice Sheet. *Science* **341**, 777–779 (2013).
35. Bartholomew, I. D. et al. Seasonal variations in Greenland Ice Sheet motion: inland extent and behaviour at higher elevations. *Earth Planet. Sci. Lett.* **307**, 271–278 (2011).
36. Stevens, L. A. et al. Greenland Ice Sheet flow response to runoff variability. *Geophys. Res. Lett.* **43**, 11295–11303 (2016).
37. Fettweis, X. et al. Reconstructions of the 1900–2015 Greenland Ice Sheet surface mass balance using the regional climate MAR model. *Cryosphere* **11**, 1015–1033 (2017).
38. Csatho, B. M. et al. Laser altimetry reveals complex pattern of Greenland Ice Sheet dynamics. *Proc. Natl Acad. Sci. USA* **111**, 18478–18483 (2014).
39. Schild, K. M. et al. Glacier calving rates due to subglacial discharge, fjord circulation, and free convection. *J. Geophys. Res. Earth Surf.* **123**, 2189–2204 (2018).
40. Moon, T. et al. Subsurface iceberg melt key to Greenland fjord freshwater budget. *Nat. Geosci.* **11**, 49–54 (2018).
41. Wadham, J. L. et al. Ice sheets matter for the global carbon cycle. *Nat. Commun.* **10**, 3567 (2019).
42. Hong, W. L. et al. Discharge of meteoric water in the Eastern Norwegian Sea since the last glacial period. *Geophys. Res. Lett.* **46**, 8194–8204 (2019).

Methods

Bedrock borehole drilling and instrumentation. The drilling and instrumentation of DH-GAP04 were carried out in June–July 2011 using double tube WL-75 (NQ-2) core drilling equipment. To drill through the permafrost and prevent the borehole from freezing up, heated drilling water (up to 60 °C) was used. The total water consumption was 535 m^3; 295 m^3 was used for drilling and 240 m^3 for keeping the borehole open until instrumentation. The completed borehole has a diameter of 75.7 mm, an inclination of 70° and a bearing of 10° relative to the north. After drilling, the borehole was hydraulically investigated using the Posiva Flow Log (PFL) method[43]. PFL measures the flow rate into or out of defined borehole sections via thermal dilution of an imposed heat pulse (test sections are kept isolated by rubber packing discs) and simultaneously measures hydraulic fracture heads, electrical conductivity in borehole water and fracture-specific water, single-point resistance of the borehole wall and temperature of the borehole water.

Working time in the borehole was limited by the permafrost conditions, thus the principal goal of the PFL measurements was to locate water-conducting fractures to facilitate optimal positioning of the downhole monitoring instrumentation. Hydraulic testing was therefore performed under transient flow conditions two days after hole completion. The specific capacity (flow rate per unit head change, $Q/\Delta h$, $m^2 s^{-1}$) of each water-conducting fracture intersecting the borehole was measured under two separate test conditions. Flow rate and head change were measured under elevated head conditions after borehole completion in the absence of pumping. Specific capacity was also measured under steady pumping conditions. Based on these two hydraulic tests, transmissivity was evaluated using the Thiem equation[44] for steady-state flow to a line sink[43]. All water-conducting fractures were observed below 400 m depth (later confirmed to be permafrost base by temperature measurements), and several flowing hydraulic features were observed between 540 and 640 m depth. Flow rates, borehole heads and calculated transmissivities for individual borehole sections are presented in Extended Data Table 1.

Based on the combined information from the basic core logging and the hydraulic measurements, downhole monitoring instrumentation that includes a double-packer assembly isolating a 10-metre-long section, was positioned between 561 and 571 m depth below the top of casing. Hence, the double packer divides the borehole into three monitoring sections (Up, Mid and Low). Pressure in each section was monitored by an absolute (total) pressure transducer (Druck PTX 1830). After the installation of the double-packer assembly, recovery of the borehole was observed as pressure drops in all three sections levelling off towards the end of September 2011. The largest pressure drop (40 m head equivalent) was observed in the Low section. In the Up and Mid sections pressures dropped by ~17 m (head equivalent). By mid-October 2011 pressure started to increase in all three sections, indicating that ambient hydraulic conditions were recorded.

Seasonal ice sheet elevation change. Seasonal elevation change from ice-flow dynamics and surface melt is measured from Global Positioning System (GPS) and automatic weather station (AWS) measurements at a site 21 km from the DH-GAP04 borehole (Fig. 1). Surface melt is measured from local elevation changes measured by a sonic ranging sensor. Elevation change from ice flow is measured using the vertical component of in-situ GPS stations, mounted on poles drilled 8–10 m into the ice[17]. Deep poles freeze to the near-surface ice and track horizontal and vertical ice motion, isolated from elevation changes due to surface melt.

The GPS time series of vertical motion can be decomposed into components reflecting strain thinning/thickening through the ice column, bed-parallel motion as the ice slides across its bed and changes in water storage in a Lagrangian coordinate system[45]. In contrast, the appropriate reference for ice-loading changes over an area of the bed is Eulerian. Thickness changes in this reference system are due to the advection of ice thickness gradients and to strain changes through the ice column.

Over the course of one year (for example, Fig. 3), the ice at the GPS site moves approximately 120 m. Changes in vertical strain averaged over the ice column are likely to be dominated by time variations and not space variations over this short length scale. Ice flows up a reverse bed slope at the site[17] and over the short length scales the surface slope is approximately flat. In this case of a flat ice surface, the bed-parallel motion measured by the GPS is equivalent to the advection of ice-thickness gradients in an Eulerian frame of reference. Thus, at the GPS site, the Lagrangian GPS vertical time series is a good approximation of ice-thickness changes in an Eulerian frame of reference.

The presented results demonstrate the interaction of ice-flow and surface mass-balance processes that lead to seasonal variations in ice thickness at a single site. Closer to the ice margin, surface melt rates can exceed 5 m yr^{-1}, and a steepening ice sheet profile enhances the advection of thickness gradients to replenish ice lost to melt. As a result, the seasonal pattern of thickening/thinning measured at our site should also persist closer to the margin, but we expect the magnitudes of seasonal change to be much larger.

Multi-annual ice sheet elevation change. Multi-annual changes in elevation over the study area were computed using a combination of optical stereo-imagery–based ArcticDEM[46] and National Aeronautics and Space Administration (NASA) Glacier and Ice Surface Topography Interferometer (GLISTIN-A)[47], which is processed from airborne radar interferometry. Temporal coverage of the ArcticDEM and GLISTIN-A data is 2011–2017 and 2016–2019, respectively. The proximity of the analysis area to the DH-GAP04 drill site (Extended Data Fig. 2) is constrained by data availability, requiring the assumption that the elevation changes 3–4 km from the site are representative of changes over the area forcing the groundwater system. As discussed in the text, this area lacks detailed constraint.

GLISTIN-A digital elevation models (DEMs) were co-registered to the area's ArcticDEM mosaic. ArcticDEM strip data were resampled to the coarser 50 m resolution of the GLISTIN-A product. Elevation uncertainties were estimated based on comparison of individual DEM results with ground control points from NASA's recent Ice, Cloud and Land Elevation Satellite mission (ICESat-2). Ground-control points were limited to those with surface slopes <15° to avoid introducing excess uncertainty to the data over the GrIS, which is characterized by low surface slope.

Estimate of the propagation length scale of a multi-decadal perturbation from ice thinning. In a simplified, diffusive system, boundary-pressure perturbations will attenuate with distance (z) following:

$$A = e^{\left(-z\sqrt{\frac{\pi}{\alpha\tau}}\right)} \quad (1)$$

where A is the amplitude attenuation ($A = 0$ is full attenuation of the signal and $A = 1$ is zero attenuation), τ is the perturbation period and α is the hydraulic diffusivity of the medium[32]. The hydraulic diffusivity in equation (1) is poorly constrained at our site, but it can be roughly estimated from two scenarios based on the observed timescales of groundwater response to ice forcing. In scenario 1, at the depth of measured groundwater head, the agreement between multi-annual ice thinning and groundwater head decline (Fig. 3) indicates that the groundwater system responds to multi-annual perturbations with little attenuation (at $z > 500$ m, $A \approx 0$ for $\tau > 1$ year). In scenario 2, diurnal groundwater variations indicate that perturbations with periods of one day propagate to depth (at $z > 500$ m, $A > 0$ for $\tau = 1$ day).

Based on the constraints set by scenarios 1 and 2, equation (1) yields hydraulic diffusivities in the order of ~1–10; values that fall within the expected range for fractured bedrock[48]. For this range of diffusivities, equation (1) shows that the e-folding length scale for the attenuation of pressure perturbations with a period of multiple decades (based on ongoing long-term mass loss observed in the western GrIS) is ~15–45 km. This simplified analysis indicates it is plausible that the pressure signal from long-term GrIS mass loss has propagated tens of kilometres in the groundwater system.

Data availability

Bedrock temperature (https://doi.org/10.1594/PANGAEA.928163) and groundwater head (https://doi.org/10.1594/PANGAEA.928193) data are both freely available without restrictions. Ice-sheet runoff data are archived by the Programme for Monitoring of the Greenland Ice Sheet (http://www.promice.org/PromiceDataPortal/), with identifiers: https://doi.org/10.22008/FK2/GUW0Y8. Ice-sheet basal water-pressure data have been previously published (https://doi.org/10.1002/2016JF003819), as have GPS data (https://doi.org/10.1126/sciadv.aaw5406).

References

43. Pöllänen, J., Heikkinen, P. & Lehtinen, A. *Difference Flow Measurements in Greenland, Drillhole DH-GAP04 in July 2011* Posiva Working Report 2012-13 (Posiva Oy, 2012).
44. Thiem, G. *Hydrologische Methoden* (Gebhardt, 1906).
45. Hooke, R. L., Calla, P., Holmlund, P., Nilsson, M. & Stroeven, A. A 3 year record of seasonal variations in surface velocity, Storglaciaren, Sweden. *J. Glaciol.* **35**, 235–247 (1989).
46. Porter, C. et al. *ArcticDEM Version 1*. Dataverse (DataVerse, 2018); https://doi.org/10.7910/DVN/OHHUKH
47. *OMG Glacial Elevations from GLISTIN-A Ver. 1* v.1 PO.DAAC (OMG, accessed 15 July 2020); https://doi.org/10.5067/OMGEV-GLNA1
48. Barbour, A. J. & Wyatt, F. K. Modeling strain and pore pressure associated with fluid extraction: the Pathfinder Ranch experiment. *J. Geophys. Res. Solid Earth* **119**, 5254–5273 (2014).

Acknowledgements

This work has been supported by the Greenland Analogue Project (GAP), the Catchment transport and Cryo-hydrology Network (CatchNet), Svensk Kärnbränslehantering AB (SKB) and National Science Foundation Office of Polar Programs–Arctic Natural Sciences award #0909495. T.M. is additionally supported by NSF-EPSCoR award 1929068 and Montana NASA EPSCoR award G185-19-W5586. K. Hansson, J. Sundberg (Geosigma) and L. Andersson (SKB) are acknowledged for field and borehole instrument support. J. Moore, B. Woessner, S. Berglund and J. Liakka are thanked for valuable comments on an early manuscript draft. B. Kurylyk and G. Clarke are thanked for detailed comments that resulted in improvements to the manuscript.

Author contributions

The study was conceived by L.C.L., J.-O.N., J.-O.S., T.R. and A.K. L.C.L., T.R. and A.K. led the bedrock borehole drilling and data collection. T.M., J.H. and N.H. completed ice-sheet borehole drilling and data collection and D.v.A. collected AWS data. J.S. completed the DEM analysis. L.C.L., T.M. and J.H. wrote the manuscript. All authors contributed to data interpretation and manuscript edits.

Competing interests

The authors declare no competing interests.

Additional information

Extended data is available for this paper at https://doi.org/10.1038/s41561-021-00813-1.

Supplementary information The online version contains supplementary material available at https://doi.org/10.1038/s41561-021-00813-1.

Correspondence and requests for materials should be addressed to Lillemor Claesson Liljedahl or Toby Meierbachtol.

Peer review information Primary handling editor: Tom Richardson. *Nature Geoscience* thanks Barret Kurylyk, Garry Clarke and the other, anonymous, reviewer(s) for their contribution to the peer review of this work.

Extended Data Table 1 | Testing results and hydraulic conditions from PFL testing at discrete intervals after borehole completion. Testing details are described in Methods; two tests in each interval are referenced with _0 and _1 identifiers. Depths are referenced to top of casing (TOC)

Section	Depth below TOC [m]	Head_0 [m]	Flow_0 [mL h^{-1}]	Flow_0 [m^3 s^{-1}]	Head_1 [m]	Flow_1 [mL h^{-1}]	Flow_1 [m^3 s^{-1}]	T [m^2 s^{-1}]	Head of fracture [m]
Up	392.3	526.41	-	-	514.35	103	2.9E-8	2.35E-09	*
	517.4	527	3340	9.3E-7	515.05	8390	2.3E-6	1.16E-07	534.9
	520.8	526.98	16300	4.5E-6	515.01	50500	1.4E-5	7.86E-07	532.69
	551.9	527.09	73500	2.0E-5	515.2	182000	5.1E-5	2.51E-06	535.14
Mid	566.7	527.23	119000	3.3E-5	515.67	257000	7.1E-5	3.29E-06	537.2
	570.2	527.18	1040	2.9E-7	515.25	3570	9.9E-7	5.82E-08	532.08*
Low	602.7	527.34	214	5.9E-8	515.43	653	1.8E-7	1.01E-08	533.15
	632.5	527.53	-	-	515.61	68	1.9E-8	1.57E-09	*
	643.8	528.1	−179**	−5.0E-8	516.25	140	3.9E-8	7.40E-09	521.45*

* Uncertain fracture. The flow rate is less than 30 ml h-1 or the flow anomalies are overlapping or unclear due to noise. ** Negative flow means flow out from the borehole.

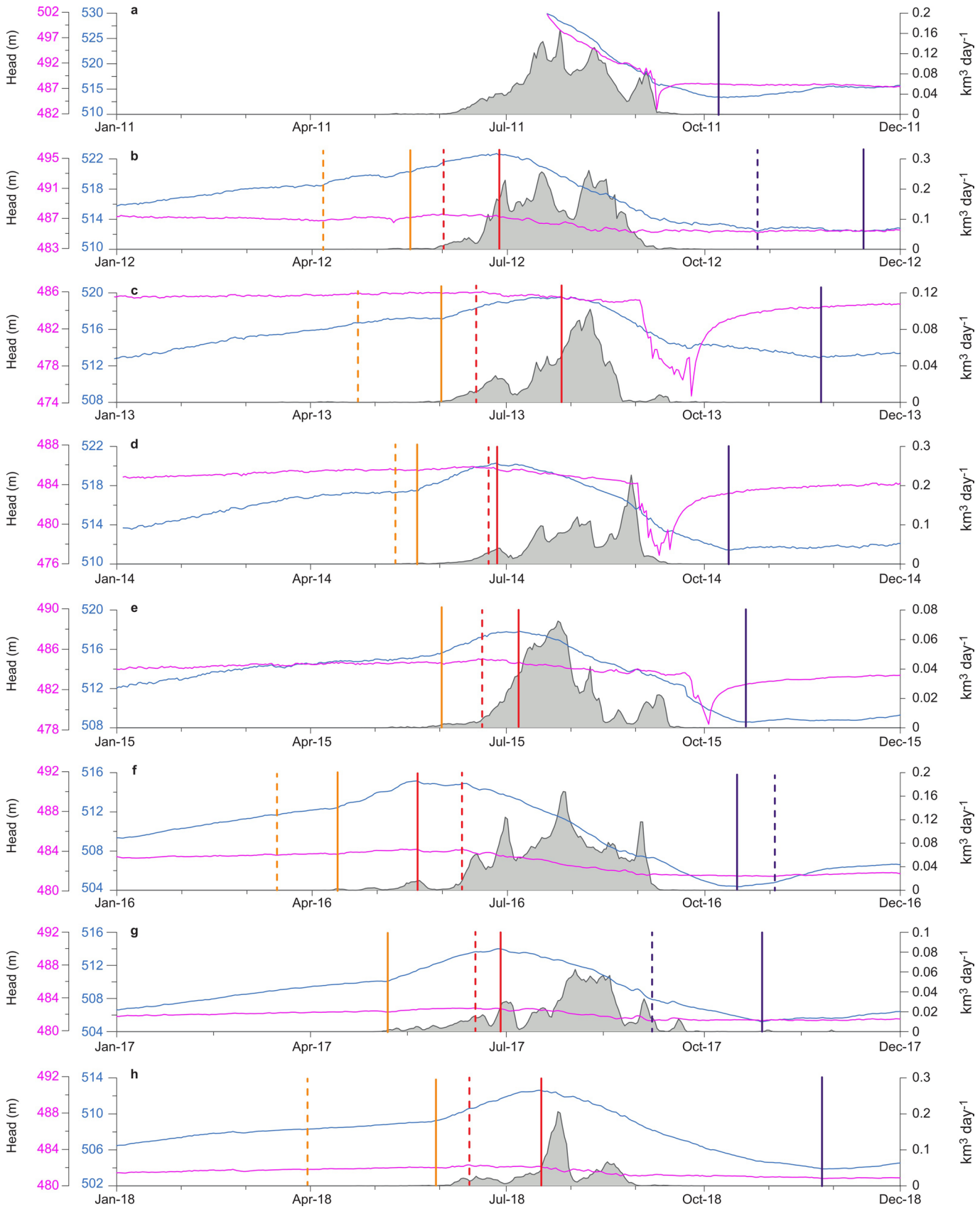

Extended Data Fig. 1 | Annual groundwater head and ice sheet runoff over eight years. a-h, Annual groundwater head in Up (blue) and Low (pink), and corresponding calculated runoff integrated over the Isunnguata Sermia catchment (gray, Supplementary Methods). Vertical lines show the transition to increasing groundwater head in spring (yellow), annual maximum head (red), and minimum head (purple) in Up (solid) and Low (dashed) sections. Years without transition lines for Low section either indicate identical timing to Up, or are obscured by pumping.

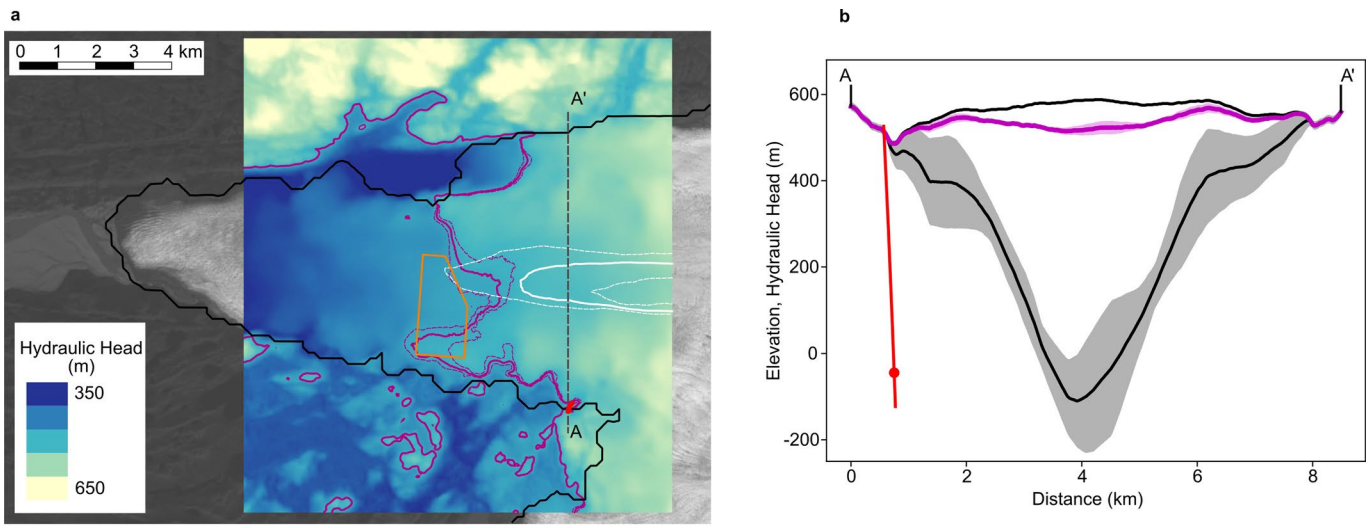

Extended Data Fig. 2 | Proglacial and subglacial hydraulic head over study area. a, Plan view of computed hydraulic head. Solid black line indicates ice sheet margin and gray dashed line (A-A') shows location of the glacier cross section in **b**. Colormap shows calculated hydraulic head in meters equivalent (Supplementary Discussion). Solid and dashed magenta lines delineate the 490 m head contour and uncertainty, respectively. This contour is presented to illustrate locations of head conditions similar to measured heads in Low. White solid and dashed lines indicate the bed elevation and uncertainty, respectively, corresponding to the elevation of the packer separating the Low section from the remainder of the borehole. **b**, Ice surface and bed topography (black) along S-N cross section intersecting bedrock borehole location. Bed topography uncertainty is shown in shaded gray. Hydraulic head and corresponding uncertainty in magenta and shaded magenta, respectively. Borehole is shown in red, with lower packer as red dot.